Evaluation of neutron-induced activation gamma-rays creation and transport in a $LaBr_3$ inorganic scintillator with PHITS

C. Besnard-Vauterin[1,*], R. De Stefano[2], G. Amoyal[2], V. Schoepff[2], J-C. Angélique[3]
[1] Université Paris-Saclay, CEA, LIST, Laboratoire National Henri Becquerel, F-91129, Palaiseau, France
[2] Université Paris-Saclay, CEA, LIST, F-91129, Palaiseau, France
[3] Normandie Univ, ENSICAEN, UNICAEN, CNRS/IN2P3, LPC Caen, 14000 Caen, France
(*) clement.besnardvauterin@cea.fr

***Abstract*—In the framework of its R&D activities to support the metal industry, the Laboratory for Integration of Systems and Technology of CEA Paris-Saclay started studies with the aim of characterizing scrap metal by means of neutron activation analysis. This involves irradiating samples of scrap metal with a pulsed-neutron source in order to determine the copper composition (mainly Cu-65 and Cu-63). In this scope, the use of a $LaBr_3$ detector with an energy resolution of 14.6 keV at 661 keV is hereby investigated to carry out acquisitions during and between the irradiation pulses. As pointed out in literature, the $LaBr_3$ inorganic scintillator might suffer some damage in a neutron-rich environment. Understanding the degradation of the energy resolution of such detector due to a high dose environment is essential to analyse the recorded signal. In this context, the work described in the present paper explores the coherent creation of neutron induced activation products as well as their respective delayed gamma rays in the quite well established LaBr3 inorganic scintillator by the mean of two steps Monte Carlo simulations performed first with the DCHAIN code, and secondly with the PHITS general purpose Monte Carlo particle transport code. Coherence was shown between neutron-induced activation gamma rays and the isotopes created in the crystal, and between the isotopes created and their decay through time. Thus, this study validate the two-step calculation scheme with PHITS and DCHAIN for both the time and energy aspects.**

***Keywords*— Neutron activation analysis, PHITS, DCHAIN.**

I. INTRODUCTION

Neutron activation analysis (NAA) is a technique widely employed for the non-destructive determination of elemental composition in various materials, including several types of radioactive waste packages but also metals. This technique involves subjecting the samples of interest to neutron irradiation, leading to the production of radioisotopes, and subsequently measuring the gamma radiation emitted during their radioactive decay. By analysing these gamma rays, valuable information regarding the elemental composition of the samples can be obtained. Neutron activation analysis finds applications in various fields due to its ability to provide accurate and precise elemental analysis. Some of the fields where NAA is predominantly used include archaeology, environmental and earth sciences, forensics, food and agriculture, nuclear science and reactor analysis, homeland security and finally material science [1].

Within the context of supporting the metal industry, the Laboratory for Integration of Systems and Technology at CEA Paris-Saclay has initiated research and development activities focused on characterizing scrap metal using neutron activation analysis [2]. This innovative approach involves subjecting samples of scrap metal to neutron irradiation using a pulsed-neutron source. The primary objective is to determine the composition of copper within the samples, with a particular focus on identifying the isotopes Cu-65 and Cu-63. By leveraging neutron activation analysis, valuable insights can be gained regarding the copper content in the scrap metal, enabling enhanced recycling processes and efficient utilization of resources.

In this context, gamma spectrometry is an extensively used tool for the identification and quantification of the radioisotopes present in the samples. $LaBr_3$ inorganic scintillators are well-established detectors for gamma spectrometry, thanks to their high light output and favourable energy resolution of 2 to 3% at 662 keV, although lower than High Purity Germanium (HPGe) detectors, which are considered the gold standard for gamma spectrometry and offer resolutions around 0.3%. $LaBr_3$ scintillators provide a compelling alternative to HPGe detectors, as they do not require cooling, are cost-effective, easily deployable, and portable. However, it has been reported in [3] that $LaBr_3$ scintillators may suffer some damage in a neutron-rich environment, which can lead to degradation of their energy resolution. Therefore, understanding the impact of neutron flux on the performance of $LaBr_3$ detectors is essential for accurate characterization of waste or metals using neutron activation analysis.

In this article, we investigate the coherent creation of neutron induced activation products as well as their respective delayed gamma rays if the $LaBr_3$ scintillators using two steps Monte Carlo simulations performed with the DCHAIN code (version 3.25) and the PHITS (version 3.27) general-purpose Monte Carlo particle transport code. DCHAIN [4, 5] is a software package designed to calculate the radioactive decay and transmutation chains of a wide range of isotopes, including fission products and actinides, produced by neutron irradiation of materials. It can also calculate the gamma-ray spectrum resulting from the decay of these isotopes, and the neutron

spectrum resulting from neutron-induced reactions. PHITS [6] is a general-purpose Monte Carlo particle transport code that simulates the interactions of various particles with matter, including neutrons, photons, electrons, and heavy ions. It can also simulate the transport of radiation through complex geometries, such as those encountered in nuclear facilities or medical applications.

Simulated results were compared with data from the Nuclear Data Sheets for bromine and lanthanum to validate the coherent calculation of neutron induced activation gamma rays [7-8-9]. There half-lives were also calculated and compared to databases [10-11].

II. METHODS AND NUMERICAL APPROACH

A detailed model of a $LaBr_3$ inorganic scintillator with dimensions of 7.62 × 7.62 cm² was implemented for this study. The scintillator crystal in the model corresponds to a cylindrical volume doped with 5% cerium, resulting in a $LaBr_3$:Ce composition. To capture the emitted light from the scintillator, a cylindrical aluminum photomultiplier (PMT) was coupled to the crystal. The PMT was depicted by a volume of 7 cm height, 3 cm radius , and 0.64 mm thickness. A one millimetre thick PVC seal joins the last two parts together. Figure 1 depicts the three-dimensional geometry of the detector, providing a visual representation of its structure.

For the material composition of the detector, the natural isotopes present in the respective elements were considered. The bromine component consisted of Br-79, which accounts for 50.69% of the natural abundance, and Br-81, which makes up the remaining 49.31%. In the case of lanthanum, the material description included La-138, which has a natural abundance of 0.09%, and La-139, which comprises 99.91% of the isotopes. Lastly, cerium was represented by the isotope Ce-140, which is present at a 100% abundance as a first approximation. By incorporating these specific isotopes into the material description, the simulation accurately reflects the natural composition of the elements used in the $LaBr_3$:Ce detector. This level of detail enhances the realism of the simulation and ensures that the generated results align as closely as possible with the characteristics and behaviour of the actual detector system.

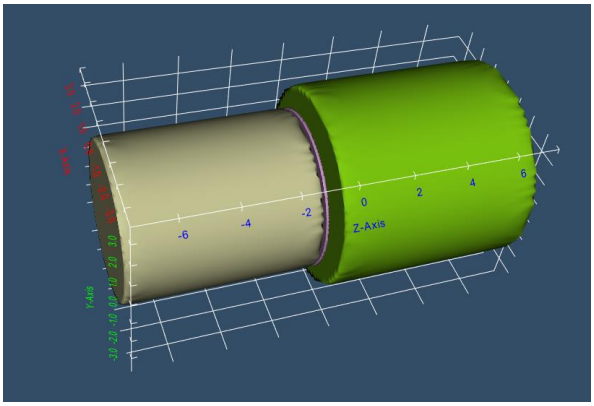

Fig. 1. 3D representation of the detector geometry where the $LaBr_3$:Ce crystal is represented in green.

In this section, we focus on analysing the activation response of a $LaBr_3$:Ce detector to neutron flux. To accomplish this, we employed a two-step approach using Monte Carlo simulations with the DCHAIN and PHITS codes. These simulations enabled us to investigate both the creation and transport of neutron-induced activation gamma-rays within the detector, as well as the subsequent decay of activation products.

Due to a limitation in the functionality of the DCHAIN code, the calculation was divided into two steps. While DCHAIN can simulate the gamma spectra resulting from the decay of activation products generated by neutrons, it provides only a description of these spectra based on energy group structures through the IGGRP (option of gamma-ray spectrum group) card output option. This limitation makes it challenging to perform a more detailed analysis of each individual gamma-ray generated in the process.

To overcome this limitation and obtain a more comprehensive understanding of the neutron-induced activation response, we incorporated the PHITS code into the workflow. The PHITS code allowed us to capture the detailed characteristics of the activation gamma-rays and their subsequent transport within the detector. By employing this two-step process, we could bridge the gap between the initial creation of activation products at different output times and their subsequent decay, enabling a more in-depth analysis of the generated gamma-ray spectra.

The flowchart presented in Figure 2 illustrates the sequential nature of this two-step process. It highlights the simulation workflow, starting with the initial creation of activation products through neutron interactions and their subsequent transport within the detector, followed by their decay and the resulting gamma-ray spectra.

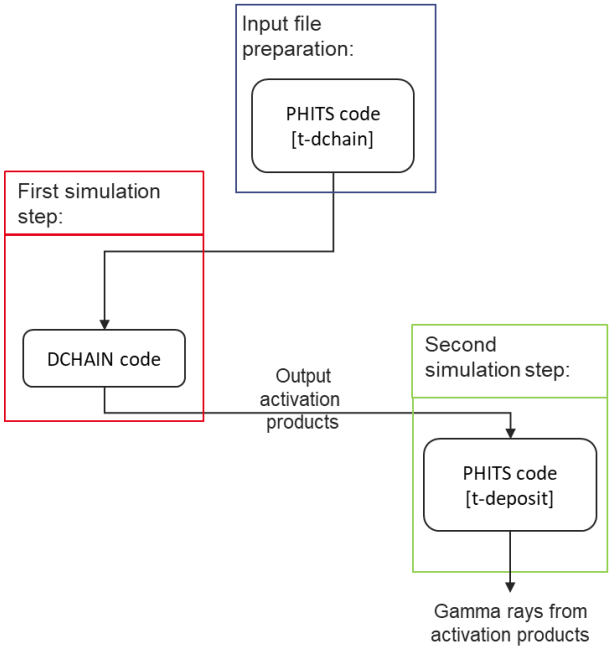

Fig. 2. Flowchart of the two-steps process for the investigation of the activation products and their decay induced by neutrons in a $LaBr_3$:Ce detector.

During the initial step, the PHITS tally [T-Dchain] was used to facilitate the generation of the required input files for the

DCHAIN code. The PHITS tally served as an automated tool, streamlining the process of file generation and ensuring the necessary files were appropriately prepared for subsequent analysis using DCHAIN.

To initiate the simulation process, a preliminary step involved subjecting the system to a 2-hour irradiation using a Cf-252 source. The source was positioned at a distance of 10 cm in front of the detector. During the irradiation, the Cf-252 source emitted neutrons with an average energy of 2.3 MeV, following a Watt spectrum. The neutron flux emitted by the source had an intensity of 2.4×10^4 neutrons per second within a 4π sr sphere.

Following the 2-hour irradiation, the subsequent step involved extracting descriptions of the created isotopes at different times over a 72-hours time period. The extracted descriptions of the isotopes were registered in a systematic manner. To provide a visual representation of the extraction process, the chronogram in Figure 3 illustrates the time intervals at which the descriptions were captured throughout the entire 72-hours period.

By conducting the simulation in this manner, the study aimed to closely monitor and analyse the behaviour of the isotopes during the phase following the initial irradiation.

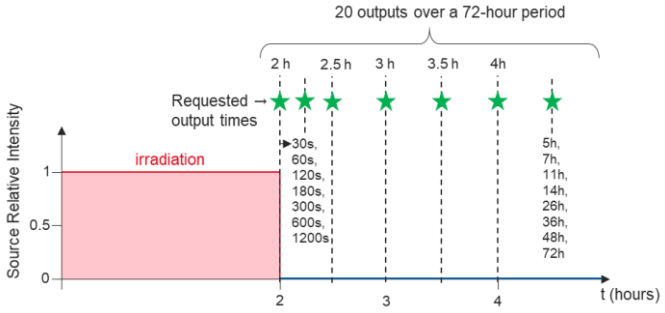

Fig. 3. Irradiation and radioactive decay monitoring chronogram.

Following the extraction of isotopic descriptions, a second calculation step was performed to consider the activated $LaBr_3$:Ce detector as a source. To achieve this, the PHITS RI-source function was employed, enabling the generation of photon sources with energy spectra corresponding to radioisotope (RI) decay. By specifying the activity and name of the radioisotopes, PHITS utilized the nuclear decay database DECDC, which is equivalent to ICRP107 [10], to accurately model the decay process.

To ensure a reliable and accurate assessment, a passive approach was adopted by simulating a second detector placed nearby the primary activated $LaBr_3$:Ce. This approach was chosen in order to limit potential effects arising from the simulation of a region used as both a source and a detector. To implement this configuration, the geometry reported in Figure 4 was employed.

In this setup, the activated primary $LaBr_3$:Ce crystal, located on the left side, emitted gamma-rays, which were then detected by the secondary $LaBr_3$:Ce crystal positioned on the right side.

The emitted gamma-rays from the activated $LaBr_3$:Ce crystal exhibited a consistent energy distribution. This indicates that there was no inherent bias introduced by considering the region as both the source and detector. The simulation accurately computed the energy distribution of the emitted photons, ensuring a reliable representation of the system's behaviour.

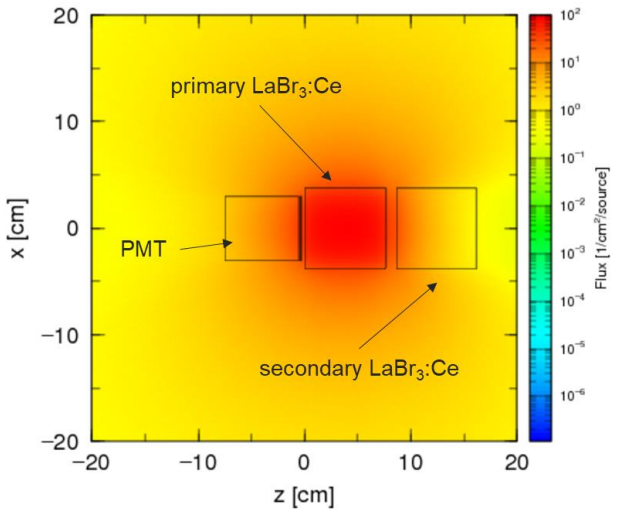

Fig. 4. Simulation of the photon mesh using PHITS [t-track] tally and showing gamma-rays emitted by the primary LaBr3:Ce after induced activation products calculated with DCHAIN where used as the source description for the second calculation step.

III. RESULTS AND DISCUSSIONS

A. Analysis of the activation gamma rays energy spectra

To illustrate the simulated gamma-ray spectrum, a specific time point of 15 seconds after the cooling phase was chosen. At this stage, the activated crystal had undergone a partial decay, resulting in a distinct gamma-ray signature. Figure 5 represents this gamma spectrum and was computed with the PHITS tally [T-Deposit] used to estimate the deposited energies in certain regions. Here it was applied to the activated crystal itself.

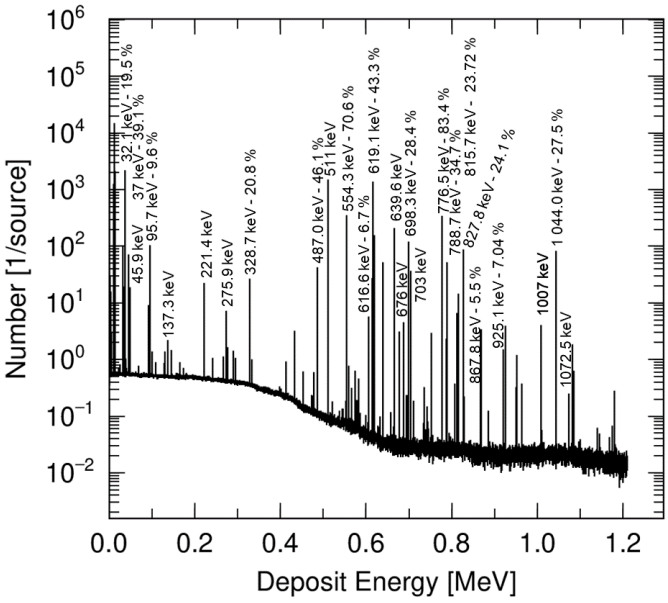

Fig. 5. Energy deposition of photons in the activated $LaBr_3$:Ce crystal without energy resolution.

Figure 6 showcases the simulated gamma spectrum after

applying the energy resolution of the $LaBr_3$ detector, which is known to be around 2.2% at 662 keV. This resolution value accounts for the inherent limitations of the detector and provides a realistic representation of the measured energy spectrum.

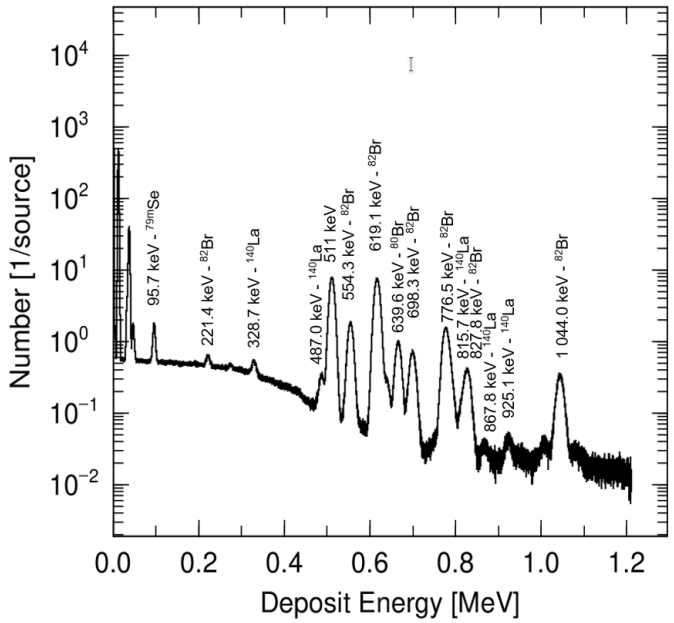

Fig. 6. Energy deposition of photons in the activated $LaBr_3$:Ce crystal taking into account its 2.2% resolution at 662 keV.

The observed spectrum exhibits several peaks corresponding to gamma-rays emitted during the decay of specific activated isotopes. For instance, among others, we can evidence a significant presence of Br-82, resulting from the (n, γ) capture of Br-81 in the spectrum. Additionally, the presence of La-140, produced through the (n, γ) capture of La-139, and Br-80, produced via the same nuclear reaction from Br-79, can be identified. Another noteworthy activation product is Se-79m, which is likely generated through the electron capture of Br-79. Those results are conform to what was reported in the publication of Y. Lu et al. [3].

B. Analysis of the temporal behaviour of the activated $LaBr_3$:Ce

By analysing the gamma-rays at different time intervals during the cooling calculation, a verification process was conducted to confirm that the decay of the activation products follows the expected Poisson law for radioactive decay (Eq. 1).

$$N(t) = N_0 . \exp(-\lambda . t) \qquad (1)$$

Where $N(t)$ represents the number of radioactive nuclei at time t, N_0 is the initial number of nuclei, λ is the decay constant, and t represents the elapsed time. This fundamental law describes the exponential decrease in the activity or number of radioactive nuclei over time. By comparing the experimental data with the expected decay behaviour following Eq. 1, the consistency and validity of the simulation results can be assessed. The decay constant is a fundamental parameter used to describe the rate at which radioactive isotopes decay. It is closely related to the concept of the half-life of decaying products. The relationship between the decay constant (λ) and the half-life ($T_{1/2}$) can be defined using the following equation:

$$\lambda = \frac{ln\,2}{T_{1/2}} \qquad (2)$$

The fitting procedure involved utilizing a negative exponential function of the form $a.\exp(-b.t)$, where ' a ' and ' b ' are parameters to be optimized, and ' t ' represents the time variable. By fitting this function to the data, the goal was to capture the underlying trends and check if the dataset was following the Poisson's law.

To quantify the uncertainties associated with the optimized parameters, the covariance matrix of the optimized parameters was used. The covariance matrix provides valuable information about the interdependencies between the parameters and their respective variances. Specifically, the diagonal elements, which represent the variances of the optimized parameters. By extracting the variances from the diagonal elements of the covariance matrix, the uncertainties associated with each parameter were calculated. In particular, the standard deviations of the parameters were determined by taking the square roots of their respective variances. It is also to mention that the statistic uncertainty for the Monte-Carlo calculations are less than 1% in most of the cases.

The estimation of parameter uncertainties is crucial in evaluating the reliability and robustness of the fitted function. These uncertainties provide insights into the sensitivity of the fitted function to changes in the input data and aid in understanding the stability and precision of the fitting procedure.

Starting with the nucleus exhibiting the shortest half-life, Figure 7 depicts the temporal evolution of gamma ray counts at 96 keV originating from Se-79m, alongside its corresponding fitted curves. The calculated half-life for Se-79m is 3 minutes and 58.47 seconds with a precision of ±1.37 seconds, while the CEA-LNHB LARA library for gamma and alpha spectrometry (Ref. [11]) lists its half-life as 3 minutes and 55.2 seconds.

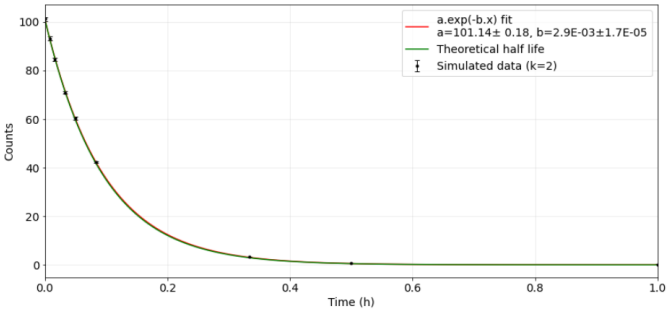

Fig. 7. Temporal variation of 96 keV gamma ray counts from Se-79m and fitted curves.

Figure 8 reports the temporal evolution of gamma ray counts at 46 keV emitted from Br-82m, complemented by fitted curves. Br-82m's calculated half-life is 6 minutes and 18.10 seconds (±3.57 seconds), while the LARA library records its

half-life as 6 minutes and 7.8 seconds.

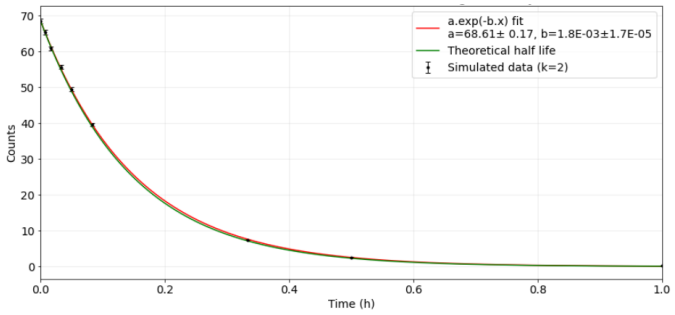

Fig. 8. Temporal behaviour of 46 keV gamma ray counts from Br-82m and fitted curves.

Figure 9 displays a distinct scenario involving the temporal behaviour of gamma ray counts at 639 keV originating from two isotopes, namely Br-80 and Br-80m. This case holds particular significance due to the contrasting half-lives of the isotopes and their decay processes. Despite Br-80m showing a longer half-life than Br-80, it assumes a crucial role in the decay chain, effectively being a precursor to the decay of Br-80. To comprehensively understand this dependence, a double exponential fit was employed, offering an analytical approach that takes into account the contributions from both Br-80 and Br-80m to the observed gamma ray counts. The derived half-life measurements for Br-80 and Br-80m were found to be 17 minutes and 41.14 seconds (±0.75 seconds) and 4 hours, 24 minutes, and 31 second (±1 minute, 15 seconds), respectively. Notably, the LARA library values for Br-80 and Br-80m were found as 17 minutes, 40.8 seconds and 4 hours, 25 minutes, 10 seconds respectively.

This particular case exemplifies the importance of carefully considering the interplay between different isotopes and their decay processes, especially when one isotope influences the decay of another. The observed temporal behaviour, coupled with distinct half-life measurements, unveils the intricacies of nuclear decay and provides valuable insights for further studies in nuclear physics and related disciplines.

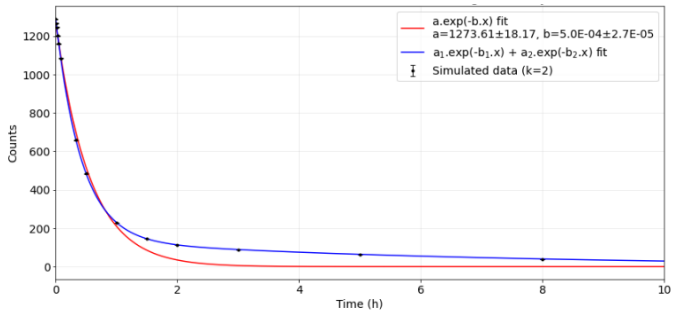

Fig. 9. Temporal behaviour of 639 keV gamma ray counts from br-80 and br-80m with fitted curves. The red curve represents a single exponential fit, inadequate to account for contributions from both isotopes.

Transitioning to isotopes with longer half-lives, Figure 10 illustrates the temporal evolution of the 221 keV gamma ray emitted by the Br-82 isotope. The calculated half-life is determined to be 36 hours, 56 minutes, and 32 seconds, accompanied by an uncertainty of 1 hour, 10 minutes, and 48 seconds. Conversely, the LARA library attributes a half-life of 35 hours, 18 minutes, and 0 seconds to Br-82.

The presence of a 4.65% relative difference between the calculated and library-based half-life values can be rationalized by statistical fluctuations occurring in the simulation data points during the initial hour after irradiation. Nevertheless, it is noteworthy that the simulation results stay in good agreement with theoretical expectations.

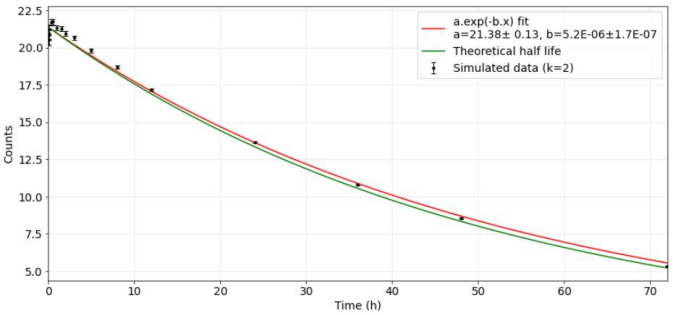

Fig. 10. Temporal behaviour of 221 keV gamma ray counts from Br-82 and fitted curves.

The La-140 isotope, so far neglected, is presented in Figure 11. The fitting procedure enables the determination of its half-life as 40 hours, 1 minute, and 43 seconds, accompanied by an uncertainty of 14 minutes and 3.97 seconds. This computed value demonstrates concordance with the LARA-based half-life of 40 hours, 17 minutes, and 9 seconds.

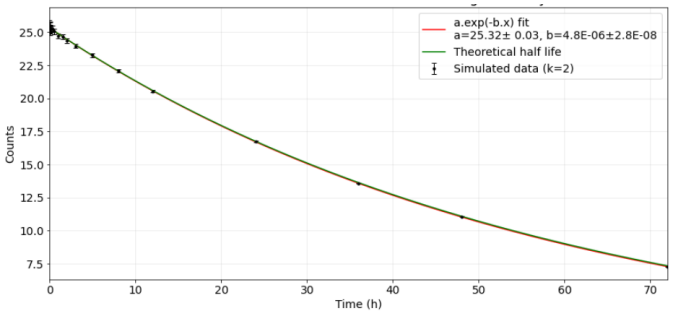

Fig. 11. Temporal behaviour of 329 keV gamma ray counts from La-140 and fitted curves.

Table I summarizes, the results of calculated half-lives based on simulations with the theoretical half-lives from the CEA-LNHB LARA library. Remarkably, a high degree of concordance is observed between the calculated and library-based half-life values, which significantly increase our confidence in the accuracy and reliability of the numerical model employed in this study.

TABLE I
COMPARISON OF CALCULATED AND THEORETICAL HALF-LIVES FOR ISOTOPES CREATED IN THE ACTIVATED $LaBr_3$

Isotopes created	Calculated half-lives	Uncertainty of the calculated half-lives	Theoretical half-life from Ref. [7]	Relative differences
Se-79m	3m 58.47s	1.37s	3m 55.20s	1.39 %
Br-82m	6m 18.10s	3.57s	6m 7.80s	2.80 %
Br-80	17m 41.14s	0.75s	17m 40.80s	0.03 %
Br-80m	4h 24m 31s	1m 15s	4h 25m 10s	0.25 %

Br-82	36h 56m 32s	1h 10m 48s	35h 18m 0s	4.65 %
La-140	24h 37m 30s	14m 3.97s	40h 17m 9s	0.64 %

We would like to emphasise that the important presence of Br-82, with a half-life of 23 hours, 2 minutes, and 22 seconds, and La-140, with a half-life of 24 hours, 37 minutes, and 30 seconds, should be acknowledged due to their relatively long half-lives. These longer-lived isotopes have the potential to contribute to the internal gamma background noise of the detector after activation especially because of the high intensity on some gamma-rays like at 1596 keV (95.4%) and 487 keV (46.1%) for LA-140 and at 776 keV (83.4%), 554 keV (70.6%) and 619 keV (43.3%) for Br-82 [11]. When the detector has been activated and these isotopes are present, the internal activity levels can remain elevated for a considerable period of time. It could take several days for the activity levels to gradually decrease and return to normal background levels. During this period, the presence of Br-82 and La-140 will contribute to the gamma radiation emitted by the detector, resulting in an increased internal gamma background noise.

It is essential to consider the impact of these longer-lived isotopes when analysing the gamma spectra obtained from the activated detector. Their presence can influence the overall detection sensitivity and may require additional data processing techniques or corrections to accurately distinguish and quantify other gamma rays of interest.

Our analysis sheds light on the effects of neutron-induced activation on the $LaBr_3$:Ce detector and validates the calculation scheme with PHITS and DCHAIN for both the energy spectra aspect and the temporal behaviour of activation gamma-rays. In addition, we discuss the implications of our findings for the accurate characterization of materials using neutron activation analysis.

IV. Conclusions

In conclusion, our study has provided valuable insights into the behaviour of $LaBr_3$ scintillators in gamma spectrometry for neutron activation analysis, particularly under neutron flux conditions. Through comprehensive simulations using the DCHAIN and PHITS codes in a two-steps process, we have demonstrated the coherence between neutron-induced activation gamma-rays, the resulting isotopes in the $LaBr_3$:Ce crystal, and their decay characteristics over time. This validation of the numerical approach consisting in the coupled use of PHITS along with DCHAIN strengthens the reliability and accuracy of calculations in this field. Moreover, our study showcases the versatility and adaptability of these codes in addressing complex research questions in the field of neutron activation analysis. It is a compelling demonstration of the correct use of the DCHAIN and PHITS codes in two-step computations.

As perspectives, it is crucial to further study and explore the combined effects of activation and (n, n'γ) reactions in the simulation and to compare those results with experimental measurements of gamma spectra in a neutron field. This will led to a better comprehension of the degradation of the energy resolution of the $LaBr_3$ scintillators when exposed to a neutron flux.

Acknowledgment

The authors gratefully acknowledge the fruitful collaboration with the PHITS team, and in particular, express their sincere appreciation to Tatsuhiko-san for his valuable support, availability, and prompt responses, which significantly contributed to this work.

References

[1] E. Witkowska, K. Szczepaniak, M. Biziuk, “Some applications of neutron activation analysis: A review”, *Journal of Radioanalytical and Nuclear Chemistry*, vol. 265, no. 1, pp. 141-150 (2005).
[2] R. De Stefano, A. Elayeb, A. Sari et al., “Evaluation of linac-based delayed gamma neutron activation technique for copper characterization in scrap metal by means of Monte Carlo modeling”, *Nucl. Inst. and Meth. in Phys. Res. Sect. A*, vol. 1045, no. 167441 (2023).
[3] Y. Lu, Z. Song, G. Li, et al., “Study of neutron radiation effect in LaBr3 scintillator”, *Chinese Phys. C*, vol. 39, no. 106003 (2015).
[4] K. Tasaka, “DCHAIN 2: A Computer Code for Calculation of Transmutation of Nuclides: Tech. Rep. JAERI-M 8727”, Japan Atomic Energy Research Inst. (1980).
[5] N. Hunter et al., “Modernization of the DCHAIN-PHITS activation code with new features and updated data libraries”, *Nucl. Inst. And Meth. in Phys. Res. B*, vol. 484, pp. 29-41 (2020).
[6] T. Sato, Y. Iwamoto, S. Hashimoto, et al., “Features of particle and heavy ion transport code system (PHITS)”, *J. Nucl. Sci. Technol*., vol. 55, no. 6, pp. 684-690 (2018),
[7] B. Singh, Nuclear Data Sheets for A = 79, *Nuclear Data Sheets*, vol. 96, np.1, pp. 1-176 (2002).
[8] Baglin, Coral M., Nuclear Data Sheets for A = 81. *Nuclear Data She*ets, vol. 109, no. 10, pp. 2257-2437 (2008).
[9] Joshi, Paresh K., et al., Nuclear Data Sheets for A = 139. *Nuclear Data Sheets*, pp. 1-292 (2016).
[10] A. Endo, Y. Yamaguchi and K.F. Eckerman, “Nuclear decay data for dosimetry calculation - Revised data of ICRP Publication 38”, JAERI 1347 (2005).
[11] Nucléide-LARA, 2018. http://www.nucleide.org/Laraweb/index.php. (Accessed 3 May 2023).